

System Noise and Accuracy of Primary Flux Density Calibrators and Scales on RadioAstron Space Telescope Data

Yu. A. Kovalev^{a, *}, A. N. Ermakov^a, V. I. Vasilkov^a, V. A. Soglasnov^a,
M. M. Lisakov^{a, b}, and Y. Y. Kovalev^{a, b, c}

^a *Astro Space Center, Lebedev Physical Institute, Russian Academy of Sciences, Moscow, 117997 Russia*

^b *Max-Planck-Institute fur Radioastronomie, Bonn, D-53121 Germany*

^c *Moscow Institute of Physics and Technology, Dolgoprudny, 141700 Russia*

*e-mail: ykovalev@asc.rssi.ru

Received May 5, 2022; revised May 23, 2022; accepted June 23, 2022

Abstract—We investigate the physical reason of the found difference in the flux density calibration for the space radio telescope on the “primary” calibrators Cassiopeia A and Crab Nebula. Twenty internal noise sources (or noise generators) of space radio telescope are analyzed as “secondary” standards measured relative to the “primary” ones in the units of the Noise Source spectral Equivalent Flux Density (in Jy). This is performed within three accurate flux density scales using monitoring data of space radio telescope calibrations at the wavelengths of 6.2, 18 and 92 cm in 2015–2018. The aims are: (1) to find and eliminate the cause of this discrepancy; (2) to propose a method for verification of flux densities of the calibrators and their scales based on the analysis of Noise Source spectral Equivalent Flux Density; (3) to analyze the System spectral Equivalent Flux Density of the space radio telescope. We have found out that the difference is a result of a variability of “primary” calibrators which is accurately quantified by the new scales proposed in 2014 and 2017. The Noise Source spectral Equivalent Flux Density measured within the new scales turned out to be more accurate than results obtained in the 1977 scale. Averaging these Noise Source spectral Equivalent Flux Density on Crab Nebula and Cassiopeia A eliminates the difference between the scales. The space radio telescope noise sources can be used to verify the quality of calibrators. An artificial standard noise source of a radio telescope can be used not only as an ordinary “secondary” calibrator but also as an indicator of relative accuracy for verifying spectral flux density calibrators and scales under certain conditions.

Keywords: methods: observational—space vehicles: instruments—radio telescopes

DOI: 10.1134/S1990341322030087

1 INTRODUCTION

Calibration is an essential procedure for converting a measurement from units in their internal representation for an individual device (including a radio telescope) into commonly used physical units. Calibrated units allow comparing measurements made by different instruments. The calibration of the radio telescope in spectral flux density units (Jy) makes calibrated results independent on the telescope, including independence on the gain and bandwidth of the receiver, the size of the telescope and its effective area. Therefore, the calibration is required for almost any operation of a radio telescope—both for a single instrument (Kuz'min and Salomonovich, 1966) and a VLBI (Matveenko et al., 1965).

It is the most convenient and easiest way to calibrate the telescope relative to strong calibration objects of small angular dimensions—relative to the width of the main lobe of the antenna pattern. However, the nature offers us in the space radio telescope (SRT) fre-

quency ranges either strong but extended or unresolved but weak calibrators. In radio astronomy practice, it has been shown that the optimal way is when the two following groups of objects are used as calibrators.

The first group consists of four strong extended “primary” flux density calibrators measured with minimal errors (Cassiopeia A, Crab Nebula, Cygnus A and Virgo A). The second group is formed by 10–20 relatively weak quasi-point “secondary” calibrators, measured relative to the “primary” calibrators. See further details in Conway et al. (1963); Kellermann (1964); Kellermann et al. (1969), which were adopted for the first time by everyone, and then Baars et al. (1977); Ivanov et al. (2018); Ott et al. (1994); Partridge et al. (2016); Perley and Butler (2013, 2017); Vinyaikin (2007, 2014, 2016).

Flux densities of the sources in both groups can vary in time. Therefore, their measurements should be periodically monitored and adjusted to enable extrapolations of the changes in flux density since the time of the original measurements. The function of a “sec-

ondary” calibrator can also be performed by a special artificial calibration signal from an internal noise generator (or a noise source, hereinafter—NS). This noise signal is injected into the input of the radio telescope receiver. Its amplitude is measured (calibrated) relative to the “primary” or “secondary” astronomical calibrator and is later used as a reference noise signal which is “always at hand” in the units of NSEFD—see, e.g., Kovalev et al. (1999).

The RadioAstron Space Radio Telescope (hereafter SRT) in flight—a paraboloid with a diameter of 10 m—operated from July 18, 2011 to January 10, 2019. It regularly observed the four “primary” calibration sources pointed above assuming the Baars et al. (1977) scale—hereafter the Baars77 scale. For the current calibrations of SRT, the measurements were mostly used relative to two of them—Cassiopeia A (Cas A) and Crab Nebula (Crab) or relative to the averaged calibrations over them—in the wavelength ranges of 1.35, 6.2, 18 and 92 cm (Kardashev et al., 2013; Kovalev et al., 2020, 2014).

The variability of Cas A and Crab, detected by Perley and Butler (2017), require additional analysis and correction of SRT flux density calibrations—from the main Baars77 scale (it was widely used for more than 40 years) to the new Perley and Butler (2017) scale (hereafter—the PB17 scale) and to the Vinyaikin (2007, 2014) scale (hereafter—the V14 scale). The variability is caused by the errors accumulated for more than 40 years and associated with the “secular” extrapolated changes in the radiation of the expanding remnants of these Supernovae.

We use the analysis below both to correct the SRT calibrations via Noise Sources in the new scales and to re-estimate the accuracy of astronomical calibrators and their scales. The article presents average 4-year monitoring results of Noise Source spectral Equivalent Flux Density (NSEFD) relative to Crab, $F_{\text{NS}}(\text{Crab})$, and to Cas A, $F_{\text{NS}}(\text{CasA})$, at the wavelength ranges 6.2, 18 and 92 cm. The results are analyzed in three flux density scales—the Baars77, PB17 and V14 scales—for each of the 20 on-board noise sources.

It is shown on the SRT data that the analysis of the NSEFD calibrated values— $F_{\text{NS}}(\text{Crab})$ and $F_{\text{NS}}(\text{CasA})$ —and their ratio

$$VR_{\text{cal}} = F_{\text{NS}}(\text{Crab})/F_{\text{NS}}(\text{CasA})$$

contains important additional information about the relative accuracy of the calibrators themselves. A noise source can be used as an indicator to check the quality of the relative “binding” of astronomical calibrators and scales to each other. In other words, the noise sources allows us to verify the calibrators and scales of spectral flux density or to verify Crab relative to Cas A in Baars77, PB17 and V14 scales in this case.

Significant systematic deviations of the test values of VR_{cal} from $1.00 \pm (1-2)\sigma$ (where σ is the random error relative to 1.00) indicate a mismatch (inaccuracy) of flux densities F_{cal} for the calibrators in this scale (as follows from our analysis of VR_{cal} for the Baars77 scale). The proximity of VR_{cal} to unity (as found for the PB17 and V14 scales) indicates the mutual agreement of F_{cal} for the calibrators and the values F_{NS} for NS in these two scales.

2. OBSERVATIONS AND CALIBRATIONS

All observations of the calibration objects were carried out in the radiometric mode of SRT as a single telescope using scanning of a source in two mutually perpendicular directions or a similar scan of an area around the source. Each receiving channel with left or right circular polarization (channels 1 or 2) had a radiometric unit with a quadratic detector at the output. At the beginning and at the end of each calibration session, successive pulses from four internal noise sources were formed in each channel: with high and low signal amplitudes (Fig. 1). The code “Hmn” of NS (where $m = 1, 2$; $n = 1, 2$) in Table 2 through Table 6 means that this is the “High”-level signal coming to a receiving channel number n from an NS located in a channel number m , and “Lmn” is the similar signal, but from an NS with the “Low”-level. As a result, each observation of a calibrator in each of the four 2-channel receivers allowed us to calibrate up to 8 main or backup NS. The examples of typical observations of calibration objects and NS at the wavelength ranges 1.35, 6.2, 18 and 92 cm can be found in Ermakov and Kovalev (2020); Kardashev et al. (2013). The NS calibrated in such sessions were later used in space VLBI sessions as “secondary” standards, relative to which System spectral Equivalent Flux Density (SEFD) of the SRT noise at different wavelengths were calibrated. The primary data processing was done in a standard way similar to processing of the ground observations — using well-known methods of least squares, Singular Value Decomposition (SVD) and weighted averaging (Ermakov and Kovalev, 2020; Forsythe et al., 1977; Kardashev et al., 2013; Kovalev et al., 2020, 2014). Further, the NS response U_{NS} (V), measured in volts after quadratic detection, was calibrated to the desired units of the spectral equivalent flux density $F_{\text{NS}}^{(0)}$ (Jy) in the Baars77 scale, using the usual relations (Kardashev et al., 2013; Kovalev et al., 1999):

$$F_{\text{NS}} = 2kT_{\text{NS}}/A_{\text{eff}} \equiv T_{\text{NS}}G_A, \quad (1)$$

$$F_{\text{NS}}^{(0)} = F_{\text{cal}}^{(0)}U_{\text{NS}}/(U_{\text{cal}}g) \equiv F_{\text{cal}}^{(0)}C_{\text{cal}}, \quad (2)$$

$$F_{\text{NS}}^{(i)} = F_{\text{NS}}^{(0)}K^{(i)}, \quad (3)$$

$$K^{(i)} = F_{\text{cal}}^{(i)}/F_{\text{cal}}^{(0)}. \quad (4)$$

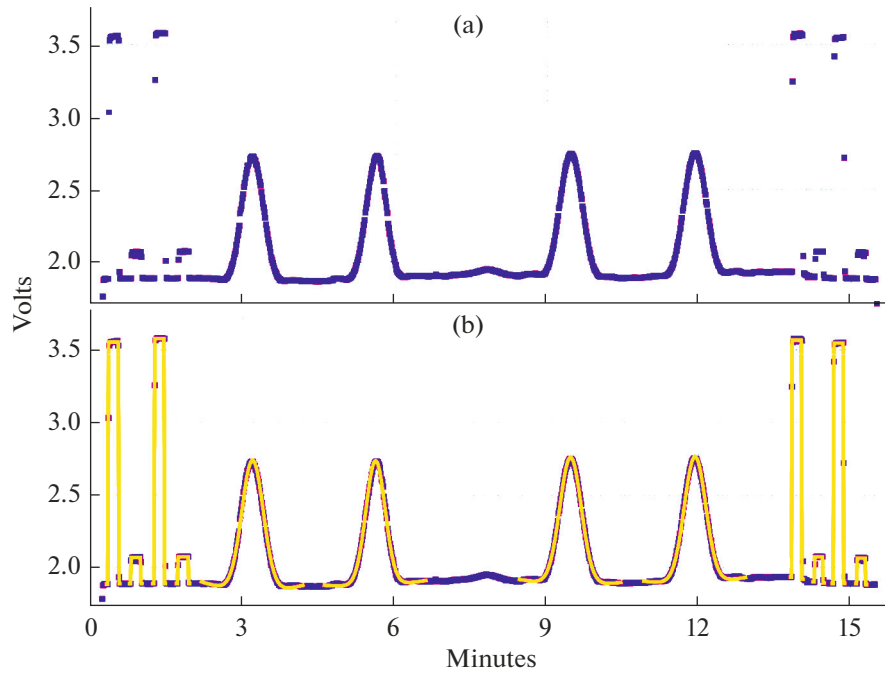


Fig. 1. (a) An example of the 18 cm record (channel 2) of Cassiopeia A observation on 29 November 2018 with SRT in flight as a single antenna which scans a source in two mutually perpendicular direction (there and back). (b) The same record with superimposed fits of model responses to the object (four responses) and to four Noise Sources (4 pulses of two high and two low amplitudes with H12, L12, H22, L22 codes at the start and end of the record).

Here, index $i = 0, 1, 2$ is used for the Baars77, PB17 and V14 scales, respectively; T_{NS} is the equivalent antenna temperature of NS, A_{eff} is the effective area of the antenna, k is the Boltzmann constant, G_A is the “antenna gain”; $F_{\text{cal}}^{(i)}$ are the flux densities (Table 1, in Jy) of Crab or Cas A, U_{cal} and U_{NS} are the SRT responses to a calibration object and to NS, respectively, measured in Volts; $C_{\text{cal}} \equiv U_{\text{NS}}/(U_{\text{cal}}g)$ does not change when the scales are replaced. The correction factor $g \geq 1$ if the partial angular resolution of the calibrator exists, $g = 1.03$ at the wavelength 6.2 cm and

$g = 1.00$ at the wavelength ranges 18 and 92 cm for Cas A and Crab.

Denote the System Equivalent Flux Density (SEFD) of the SRT system noise as F_{sys} and set $g = 1$. Then equations (1)–(3) will be valid for calibrations of F_{sys} , if all subscripts “NS” are replaced by “sys”.

It is more convenient to recalculate the units from NSEFD, F_{NS} in Jy, to T_{NS} in K. We use the SRT antenna gain G_A equal to 78.86, 67.32, and 92.00 Jy K^{-1} , according to Kovalev et al. (2014) at the wavelength ranges 6.2, 18, and 92 cm, respectively. From equations (1)–(4) also follows the way of recalculation for calibrations of $F_{\text{NS}}^{(i)}$ from the initial “base” Baars77 scale (at $i = 0$) to other analyzed scales (at $i = 1, 2$)—see equations (3) and (4) and Tables 2, 3 and 4 below.

3. RESULTS

The results of processing observations at the wavelength ranges 6.2, 18 and 92 cm during four years of monitoring and calibration of the SRT system noise and all internal noise sources measured relative to Cas A and Crab are given in Ermakov et al. (2021); Kovalev et al. (2020). The basic flux density calibration scale used was the Baars77 scale. The spectral flux densities $F_{\text{cal}}^{(i)}$ in equation (2) for Cas A and Crab in three scales and their ratios $K^{(i)}$ in equations (3) and

Table 1. Spectral flux densities F_{cal} (Jy) of Cassiopeia A (Cas A) and Crab Nebula (Crab) in the Baars77 (B77 in the table), PB17 and V14 scales; ratios $K^{(2)}$ and $K^{(1)}$ in equation (4) for the V14 and PB17 scales to the Baars77 scale, respectively (two lines)

Scale,	Cas A	Crab	Cas A	Crab	Cas A	Crab
$K^{(i)}$	6.2 cm		18 cm		92 cm	
V14	670	630	1488	815	5209	1211
PB17	639	574	1548	795	5325	1134
B77	587	651	1241	895	3877	1259
$K^{(2)}$	1.1414	0.9677	1.1990	0.9106	1.3436	0.9619
$K^{(1)}$	1.0886	0.8817	1.2474	0.8883	1.3735	0.9007

(4) are shown in Table 1 for the epoch of 2015.5. The main calibration results for the 20 NS averaged over these 4-years are summarized in Table 2 for the Baars77 scale ($i = 0$).

The percent errors in Table 2 are the random errors of T_{NS} without taking into account the errors of flux density measurements of the “primary” calibrators in the Baars77 scale. Thus, Tables 1 and 2 contain the initial results of the NS calibrations for further analysis. The results of data recalculation from Table 2 via $K^{(1)}$ and $K^{(2)}$ are shown in Table 3 (for the PB17 scale) and Table 4 (for the V14 scale) in the same format and errors as the original calibration data in Table 2 for the base Baars77 scale. It is apparent immediately from Tables 3 and 4 that at each wavelength the values of T_{NS} based on Cas A and Crab observations are more consistent than in Table 2.

Table 5 presents the calibrator verification ratios $VR_{\text{cal}}^{(i)}$:

$$VR_{\text{cal}}^{(i)} = T_{\text{NS}}^{(i)}(\text{Crab}) / T_{\text{NS}}^{(i)}(\text{CasA}), \quad (5)$$

where $T_{\text{NS}}^{(i)}(\text{Crab})$ and $T_{\text{NS}}^{(i)}(\text{CasA})$ are $T_{\text{NS}}^{(i)}$ measured relative to Crab and to Cas A using the corresponding data in Tables 2, 3 and 4 in the Baars77 ($i = 0$), PB17 ($i = 1$) and V14 ($i = 2$) scales. Random errors were estimated using the law of propagation of the average error. One-sided S estimates of dominant systematic errors can be done as $S \approx VR_{\text{cal}}^{(i)} - 1.00$.

Table 6 contains mean arithmetic values $T12_{\text{NS}}^{(i)}$ of NS antenna temperatures averaged over two calibrators in the i -scale:

$$T12_{\text{NS}}^{(i)} = [T_{\text{NS}}^{(i)}(\text{Crab}) + T_{\text{NS}}^{(i)}(\text{CasA})] / 2.$$

Their errors can include both systematic and random errors as

$$\sigma 12^{(i)} = |T_{\text{NS}}^{(i)}(\text{Crab}) - T_{\text{NS}}^{(i)}(\text{CasA})| / 2.$$

Table 7 summaries the data on the SRT system noise temperatures T_{sys} measured relative to Cas A and Crab. The data are shown for the channel 1 and 2 at the each wavelengths in the lines with the codes “B77-1” and “B77-2”, respectively. These T_{sys} are averaged over the 4-years at the Baars77 scale (Kovalev et al., 2020). The line with the code “B77-R12” gives the ratio of $R12 = T_{\text{sys}}(\text{Crab}) / T_{\text{sys}}(\text{CasA})$ in the B77 scale: in the “Cas A” column for the channel 1 (on the data in the “B77-1”-line) and in the “Crab” column for the channel 2 (on the data in the “B77-2”-line). The same, analogically—in the next lines for the PB17 and V14 scales.

Table 2. Average antenna temperature T_{NS} (K) for each of the 20 Noise Sources (NS) based on the 4-years monitoring measurements with SRT at the wavelength ranges 6.2, 18 and 92 cm in 2015–2018. The NS is calibrated relative to Cas A and Crab in the standard “primary” Baars77 spectral flux density scale. The random percent errors are indicated after the “/” symbol (Kovalev et al., 2020)

B77 scale	Cas A	Crab	Cas A	Crab	Cas A	Crab
NS code	6.2 cm		18 cm		92 cm	
H11	156/2	196/2	33.3/1	45.7/1	42.9/1	63.2/1
L11	7.04/1	8.83/2	3.54/1	4.87/1	4.28/1	6.65/4
H12	298/4	398/2	33.7/1	46.6/1	49.9/1	72.5/1
L12	11.0/3	14.4/1	3.67/1	5.09/1	5.34/2	7.76/1
H21	126/2	158/2	33.8/1	46.3/1	–	–
L21	9.31/1	11.6/2	3.62/1	4.96/1	–	–
H22	257/4	346/2	34.3/1	47.2/1	–	–
L22	16.6/3	22.2/1	3.74/1	5.16/1	–	–

Table 3. Average antenna temperature T_{NS} (K) as in Table 2 but recalibrated from the Baars77 scale to the PB17 scale via the data in Table 1

PB17 scale	Cas A	Crab	Cas A	Crab	Cas A	Crab
NS code	6.2 cm		18 cm		92 cm	
H11	170/2	173/2	41.5/1	40.6/1	58.9/1	56.9/1
L11	7.67/1	7.79/2	4.41/1	4.33/1	5.88/1	5.98/4
H12	324/4	351/2	42.0/1	41.4/1	68.6/1	65.2/1
L12	12.0/3	12.7/1	4.58/1	4.52/1	7.33/2	6.98/1
H21	137/2	139/2	42.1/1	41.1/1	–	–
L21	10.1/1	10.2/2	4.51/1	4.41/1	–	–
H22	280/4	305/2	42.8/1	41.9/1	–	–
L22	18.1/3	19.6/1	4.66/1	4.58/1	–	–

Table 4. Average antenna temperature T_{NS} (K), as in Table 2 but recalibrated from the Baars77 scale to the V14 scale via the data in Table 1

V14scale	CasA	Crab	CasA	Crab	CasA	Crab
NScode	6.2 cm		18 cm		92 cm	
H11	178/2	190/2	39.9/1	41.6/1	57.7/1	60.8/1
L11	8.03/1	8.54/2	4.24/1	4.43/1	5.75/1	6.40/4
H12	340/4	385/2	40.4/1	42.4/1	67.1/1	69.7/1
L12	12.6/3	13.9/1	4.40/1	4.63/1	7.18/2	7.46/1
H21	144/2	152/2	40.5/1	42.2/1	–	–
L21	10.6/1	11.2/2	4.34/1	4.52/1	–	–
H22	293/4	335/2	41.1/1	43.0/1	–	–
L22	18.9/3	21.5/1	4.48/1	4.70/1	–	–

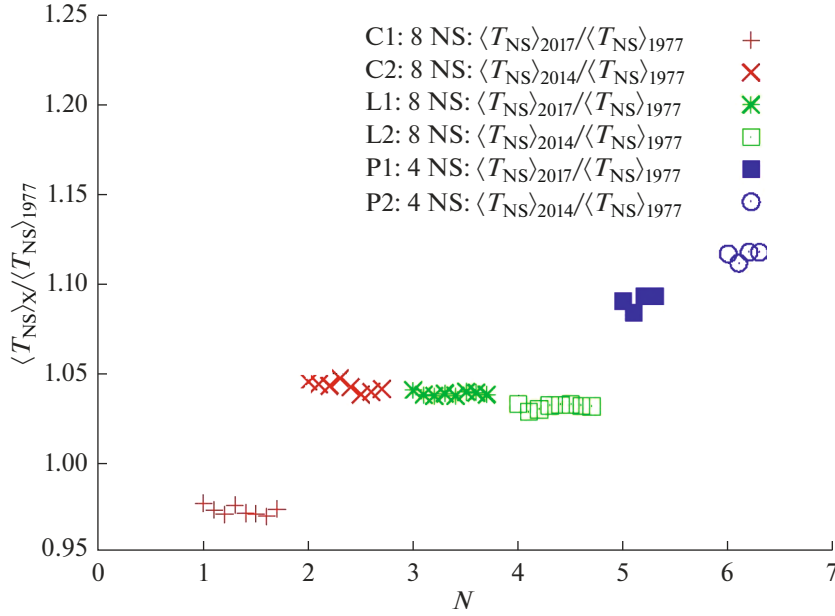


Fig. 2. Verification of accuracy of the PB17 and V14 scales relative to the Baars77 scale using the ratios $VR_{\text{scale}}^{(i,0)} = T12_{\text{NS}}^{(i)} / T12_{\text{NS}}^{(0)}$ for channels 1, 2 at wavelengths of 6.2 (C1, C2: $1 \leq N < 3$), 18 (L1, L2: $3 \leq N < 5$) and 92 cm (P1, P2: $5 \leq N < 7$). NS temperatures $\langle T_{\text{NS}} \rangle \equiv T12_{\text{NS}}$ are from Table 6.

Figure 2 shows the scale verification ratios $VR_{\text{scale}}^{(i,0)}$ of $T12_{\text{NS}}^{(i)}$ in the PB17 and V14 scales to $T12_{\text{NS}}^{(0)}$ in the Baars77 scale using the data in Table 6:

$$VR_{\text{scale}}^{(i,0)} = T12_{\text{NS}}^{(i)} / T12_{\text{NS}}^{(0)}. \quad (6)$$

The way for estimating the errors for equation (6) is similar to that of equation (5).

4. DISCUSSION

The strong discrepancy of T_{NS} relative to Crab and Cas A in Table 2 is detected in the Baars77 scale. But these T_{NS} should be almost the same from equation (1) within random errors. The discrepancy may also indicate the presence of systematic errors because of the inaccuracy or variability of F_{cal} of the calibrators in equation (2) and in Table 1 in the line with code B77. The significantly different picture is observed after the transition from the Baars77 to PB17 and V14 scales in Tables 3 and 4. F_{cal} for Cas A and Crab in Table 1 were corrected for their variability due to new measurements of these calibrators relative to Cygnus A in the PB17 and V14 scales. In contrast to Table 2, the corrected values of T_{NS} relative to Cas A and Crab in Tables 3 and 4 become close to each other for the same NS-codes and wavelengths.

So, the values of F_{NS} measured relative to the calibrators by equation (2)–(4) should coincide with each other and with the theoretical value by equation (1) (within the measurement errors). This conclusion follows from equations (1) and (2), if we consider

$T_{\text{NS}} = P_{\text{NS}} / 2kB = \text{const}$ with constancy NS power $P_{\text{NS}} = \text{const}$ and frequency bandwidth $B = \text{const}$ of the receiver. The constancy of F_{NS} implies the constancy of T_{NS} and A_{eff} also. But the condition $F_{\text{NS}} = \text{const}$ is violated if calibrators with inaccurate flux densities in equation (2) are used for NS (as a result of calibrators variability, for example) or if T_{NS} or A_{eff} are not constant.

This can be seen from the following reasoning. We denote by the lower indices 1 and 2 the values obtained relative to Cas A and Crab, respectively. Then, the theoretical T_R - and the measured $M_R^{(i)}$ -ratios of F_{NS} follow from equations (1) and (2)–(4), respectively:

$$\frac{F_{\text{NS}}(\text{Crab})}{F_{\text{NS}}(\text{Cas A})} \equiv \left(\frac{F_{\text{NS},2}}{F_{\text{NS},1}} \right)_{\text{th}} = \frac{T_{\text{NS},2}}{T_{\text{NS},1}} \times \frac{A_{\text{eff},1}}{A_{\text{eff},2}} \equiv T_R, \quad (7)$$

$$\left(\frac{F_{\text{NS},2}^{(i)}}{F_{\text{NS},1}^{(i)}} \right)_m = \frac{F_{\text{cal},2}^{(i)}}{F_{\text{cal},1}^{(i)}} \times \frac{C_{\text{cal},2}}{C_{\text{cal},1}} \equiv M_R^{(i)}. \quad (8)$$

$T_R = 1$ for SRT. Then, the ratio equation (8) has to be equal to $M_R^{(i)} = 1$ also. However, this will be the case if only some of the values of $F_{\text{cal},2}^{(i)}$ and $F_{\text{cal},1}^{(i)}$ are absolutely exact. Else they will be in disagreement with the response ($U_{\text{cal}} g$) in equations (2)–(4).

The closer the ratio VR_{cal} of T_{NS} in Table 5, obtained via Crab and via Cas A, to $1.00 \pm (1-2)\sigma^{(i)}$ in the columns of this table, the more accurate is the cal-

Table 5. Verification of accuracy of two calibrators—Cas A and Crab—for estimations of mutual consistency of their spectral flux densities F_{cal} using all Noise Sources as accuracy indicators at the wavelength ranges 6.2, 18 and 92 cm in the Baars77, PB17 and V14 spectral flux density scales. The percent random errors σ are shown after the symbols “/”. The deviations of VR_{cal} from 1.00 characterizes one-sided systematic errors of spectral flux densities F_{cal}

Ratio	$VR_{\text{cal}} = T_{\text{NS}}(\text{Crab}) / T_{\text{NS}}(\text{CasA})$								
Wavelengths	6.2 cm			18 cm			92 cm		
Noise source code	Baars77	PB17	V14	Baars77	PB17	V14	Baars77	PB17	V14
H11	1.26/3	1.02/3	1.08/3	1.37/1	0.98/1	1.05/1	1.47/1	0.96/1	1.06/1
L11	1.25/2	1.01/2	1.07/2	1.38/1	0.98/1	1.06/1	1.55/4	1.02/4	1.12/4
H12	1.34/4	1.09/4	1.15/4	1.38/1	0.98/1	1.06/1	1.45/1	0.95/1	1.05/1
L12	1.31/3	1.06/3	1.12/3	1.38/1	0.98/1	1.06/1	1.45/2	0.95/2	1.05/2
H21	1.25/3	1.01/3	1.07/3	1.37/1	0.98/1	1.05/1	—	—	—
L21	1.25/2	1.01/2	1.07/2	1.37/1	0.98/1	1.05/1	—	—	—
H22	1.35/4	1.09/4	1.16/4	1.38/1	0.98/1	1.06/1	—	—	—
L22	1.34/3	1.09/3	1.15/3	1.38/1	0.98/1	1.06/1	—	—	—

Table 6. Noise Source mean antenna temperatures $T12_{\text{NS}}$ averaged between T_{NS} relative to Cas A and Crab in Tables 2, 3 and 4 for the Baars77, PB17 and V14 scales, respectively, and estimations of total classic systematic and random percent errors $\sigma12$ (after the “/” symbol)

Average	$T12_{\text{NS}} = (T_{\text{NS}}(\text{Crab}) + T_{\text{NS}}(\text{CasA})) / 2, \text{K}$								
Wavelengths	6.2 cm			18 cm			92 cm		
Noise source code	Baars77	PB17	V14	Baars77	PB17	V14	Baars77	PB17	V14
H11	176/11	172/1	184/3	39.5/16	41.1/1	40.8/2	53.1/19	57.9/2	59.3/3
L11	7.94/11	7.73/1	8.29/3	4.21/16	4.37/1	4.33/2	5.47/22	5.93/1	6.08/5
H12	348/14	338/4	363/6	40.2/16	41.7/1	41.4/2	61.2/18	66.9/3	68.4/2
L12	12.7/13	12.4/3	13.3/5	4.38/16	4.55/1	4.52/3	6.55/18	7.16/2	7.32/2
H21	142/11	138/1	148/3	40.1/16	41.6/1	41.4/2	—	—	—
L21	10.5/11	10.2/1	10.9/3	4.29/16	4.46/1	4.43/2	—	—	—
H22	302/15	293/4	314/7	40.8/16	42.4/1	42.1/2	—	—	—
L22	19.4/14	18.9/4	20.2/6	4.45/16	4.62/1	4.59/2	—	—	—

ibration of NS and SRT and the better fluxes F_{cal} of these calibrators are consistent in the given scale. Analysing the deviations of the results for VR_{cal} in Table 5 from $1.00 \pm (1-2)\sigma^{(i)}$, it can be seen that the systematic errors of the verification ratio of equation (5) in the V14 scale are ordinary greater than in the PB17 scale but significantly less than in the Baars77 scale. Nevertheless, the differences between the Baars77 scale and the PB17 and V14 scales practically disappear if we use the averaged calibrations of NS on Crab and Cas A. It can be seen from the data in Table 6 or Fig. 2. The deviation of $VR_{\text{scale}}^{(i,0)}$ from 1.00 on Fig. 2 characterizes the inaccuracy of the scales.

The SRT system noises after averaging on Cas A and Crab for the channels 1 and 2 in Table 7 in the

Baars77 scale are in agreement with the system noises obtained in 2011–2013 in Table 1 on calibrators by Kovalev et al. (2014): the differences are 22% for the channel 1 at the wavelength 6.2 cm and less than 5% for any channels at the wavelength ranges 18 and 92 cm. The sky noises $T_{\text{sky}} \sim 120 \text{ K}$ around the calibrators are not excluded in these tables at 92 cm (see the Section 3.1.1 in Kovalev et al. (2014)).

If T_{NS} and A_{eff} in equation (1) are constant, then F_{NS} is also constant. Then this method “works”. Otherwise, it does not work or requires corrections. For SRT, both conditions (to T_{NS} and A_{eff}) are met with good accuracy. The arguments are: (1) the recalculation of F_{cal} in Table 1 to the new scales give the positive effect; (2) T_{NS} in Table 2, 3, 4 have small errors under

Table 7. System noise temperature T_{sys} for the channels 1 and 2 averaged on the 4-years monitoring measurements with SRT at the wavelength ranges 6.2, 18 and 92 cm in 2015–2018. T_{sys} for the first three lines is calibrated relative to Cas A and Crab in the Baars77 scale (Kovalev et al., 2020). T_{sys} for the second and third three lines are recalculated to the PB17 and V14 scales via the data in the first two lines here and in Table 1. The random percent errors are indicated after the “/” symbol

T_{sys} , K	CasA	Crab	CasA	Crab	CasA	Crab
Scale-R12	6.2 cm	6.2 cm	18 cm	18 cm	92 cm	92 cm
B77-1	144/3	179/3	39/2	51/2	204/2	269/3
B77-2	174/2	218/3	40/2	54/2	186/2	245/4
B77-R12	1.24/4	1.25/4	1.31/3	1.35/3	1.32/3	1.32/5
PB17-1	157/3	159/3	48.6/2	45.3/2	280/2	242/3
PB17-2	189/2	194/3	49.9/2	48.0/2	255/2	221/4
PB17-R12	1.01/4	1.03/4	0.93/3	0.96/3	0.86/3	0.87/5
V14-1	164/3	173/3	46.8/2	46.4/2	274/2	259/3
V14-2	199/2	211/3	48.0/2	49.2/2	250/2	236/4
V14-R12	1.05/4	1.06/4	0.99/3	1.03/3	0.95/3	0.94/5

similar conditions of measurements for both calibrators; (3) we see no reasons for a systematic change of T_{NS} or G_A between the directions to Cas A and Crab in absence of gravitational deformations and taking into account the SRT thermal stabilization by Tulin et al. (2014) as well as the presence of residual tension forces of the antenna petals through the cable and the thrust of the mirror opening mechanism (Kovalev et al., 2014).

Therefore, the verification of the flux density of calibrators by comparing F_{NS} calibrated via them, can be carried out quite simply for SRT. For many ground-based telescopes, this may not be the case,—at least, for A_{eff} of large telescopes (due to a dependence of A_{eff} on elevation). Then it will be more difficult to apply a similar approach to them. However, if the regularity of changes in A_{eff} is known, then such a telescope can also implement the verification by this method.

5. SUMMARY

(1) The system noises of SRT are stable between 2011–2013 and 2015–2018. Their differences are about 22% at the wavelength 6.2 cm and less than 5% at the wavelength ranges 18 and 92 cm.

(2) Usually Noise Source (NS) is used only for calibration of a receiver or a telescope. It is shown that the NS calibrations relative to two or more astronom-

ical calibrators contain additional information—about the mutual consistency or inaccuracy of spectral flux density of the calibrators. NS of a radio telescope has the spectral equivalent flux density, in Jy, $F_{\text{NS}} = 2kT_{\text{NS}}/A_{\text{eff}}$. The F_{NS} value can be constant under certain conditions, which are determined by the telescope (via the effective area A_{eff}) and by the NS power (via the antenna temperature T_{NS}). F_{NS} does not depend on the spectral flux density of a calibrator. The space radio telescope is not prone to strong gravitational and thermal deformations, hence A_{eff} can be constant, in general. T_{NS} of the used noise sources is observed to be stable during the considered time period.

(3) The proposed method considers a noise source not only as an internal calibration standard for a radio telescope but also as an indicator of the relative accuracy (the mutual mismatch) of “tabular” flux densities for astronomical calibrators,—Cas A and Crab in the given case. The method was tested at the wavelength ranges 6.2, 18 and 92 cm on the data of 4-year monitoring of the SRT calibrations.

(4) The calibration results for 20 Noise Sources relative to Cas A and Crab were analyzed in three accurate astronomical scales of spectral flux density: (1) in the standard scale relative to Cas A (the Baars et al. (1977) scale), and (2) in two scales corrected and constructed relative to Cygnus A—in the Perley and Butler (2017) scale and the Vinyaikin (2014) scales.

(5) The maximum relative total errors of the verification of Cas A and Crab including systematic and random components in three scales can be estimated in 2015–2018 from Table 5 as follows: (1) 4.5, 1 and 2.5% in the PB17 scale (Perley and Butler, 2017), (2) 8, 3 and 6% in the V14 scale (Vinyaikin 2007, 2014), (3) 18, 19 and 28% in the Baars77 scale (Baars et al. 1977) at the wavelength ranges 6.2, 18 and 92 cm, respectively. The PB17 and V14 scales are the most accurate and provide consistent results in the given time interval.

(6) The SRT calibrations relative to Cas A or Crab required recalculation of the calibrations from the Baars77 scale to the PB17 or V14 scales to eliminate systematic errors of the Baars77 scale caused by the long-term secular variability of these calibrators (see Tables 1 through 5 and Fig. 2). However, the difference between the results in the Baars77 scale and in the PB17 and V14 scales in 2015–2018 almost disappears if the NS calibrations are additionally averaged between Crab and Cas A. This difference can be estimated from Fig. 2 as 3–4% at the wavelength ranges 6.2 and 18 cm and as 9–13% at the wavelength 92 cm.

(7) For effective use of the method proposed, a telescope is needed with a constant effective area and a constant NS power (like SRT) or data on their changes. A similar verification method can be also applied to a system of 10–20 “secondary” flux density

calibrators which are used at various fully-steerable radio telescopes in the scales by Ivanov et al. (2018); Ott et al. (1994); Perley and Butler (2013, 2017) if the calibrators are verifying on the same height.

ACKNOWLEDGMENTS

The RadioAstron project is led by the Astro Space Center of the Lebedev Physical Institute of the Russian Academy of Sciences and the Lavochkin Scientific and Production Association under a contract with the Russian Federal Space Agency, in collaboration with partner organizations in Russia and other countries. The authors are grateful to Nikolai Kardashev without whom the RadioAstron project and this work would have been impossible, Evgeni Vinyaikin, Kenneth Kellermann, Ismail Rakhimov and Dmitri Skulachev for discussing the issues of SRT calibrations and Mikhail Popov for his constructive feedback. We thank Elena Bazanova for English language editing and proof-reading of the text.

FUNDING

This work was supported by the Russian Science Foundation, grant 21-12-00241.

CONFLICT OF INTERESTS

The authors declare no conflict of interest.

REFERENCES

1. J. W. M. Baars, R. Genzel, I. I. K. Pauliny-Toth, and A. Witzel, *Astron. and Astrophys.* **61**, 99 (1977).
2. R. G. Conway, K. I. Kellermann, and R. J. Long, *Monthly Notices Royal Astron. Soc.* **125**, 261 (1963).
3. A. N. Ermakov and Yu. A. Kovalev, *Transactions Inst. Applied Astronomy RAS* **54**, 21 (2020).
4. A. N. Ermakov, Y. A. Kovalev, and V. I. Vasil'kov, in *Proc. XVIII Young Scientists Conf. on Fundamental and Applied Space Researchers*, Moscow, Russia, 2021, Ed. by A. M. Sadovski, pp. 31–45 (IKI RAS, Moscow, 2021).
5. G. E. Forsythe, M. A. Malcolm, and C. B. Moler, *Computer methods for mathematical computations* (Prentice-Hall, Inc., Englewood Cliffs, 1977).
6. V. P. Ivanov, A. V. Ipatov, I. A. Rakhimov, et al., *Astronomy Reports* **62** (9), 574 (2018).
7. N. S. Kardashev, V. V. Khartov, V. V. Abramov, et al., *Astronomy Reports* **57** (3), 153 (2013).
8. K. I. Kellermann, *Astrophys. J.* **140**, 969 (1964).
9. K. I. Kellermann, I. I. K. Pauliny-Toth, and P. J. S. Williams, *Astrophys. J.* **157**, 1 (1969).
10. Y. A. Kovalev, V. I. Vasil'kov, A. N. Ermakov, et al., *Transactions of IAA RAS* **54**, 32 (2020).
11. Y. A. Kovalev, V. I. Vasil'kov, M. V. Popov, et al., *Cosmic Research* **52** (5), 393 (2014).
12. Y. Y. Kovalev, N. A. Nizhelsky, Y. A. Kovalev, et al., *Astron. and Astrophys. Suppl.* **139**, 545 (1999).
13. A. D. Kuz'min and A. E. Salomonovich, *Radioastronomical methods of antenna measurements* (New York, Academic Press, 1966).
14. L. I. Matveenko, N. S. Kardashev, and G. B. Sholomitskii, *Radiophysics and Quantum Electronics* **8** (4), 461 (1965).
15. M. Ott, A. Witzel, A. Quirrenbach, et al., *Astron. and Astrophys.* **284**, 331 (1994).
16. B. Partridge, M. López-Caniego, R. A. Perley, et al., *Astrophys. J.* **821** (1), id. 61 (2016).
17. R. A. Perley and B. J. Butler, *Astrophys. J. Suppl.* **204** (2), id. 19 (2013).
18. R. A. Perley and B. J. Butler, *Astrophys. J. Suppl.* **230** (1), id. 7 (2017).
19. D. V. Tulin, I. S. Vinogradov, A. F. Shabarchin, et al., *Cosmic Research* **52** (5), 386 (2014).
20. E. N. Vinyaikin, *Astronomy Reports* **51** (7), 570 (2007).
21. E. N. Vinyaikin, *Astronomy Reports* **58** (9), 626 (2014).
22. E. N. Vinyaikin, *Astronomy Reports* **60** (8), 744 (2016).